Journal of Food Engineering 388 (2025) 112371

Contents lists available at ScienceDirect

Journal of Food Engineering

journal homepage: www.elsevier.com/locate/jfoodeng

3D-printed gummies with programmable internal voids as delivery systems for customized amounts of micronutrients

Adrián Matas-Gil [a], Antonio Derossi [b,*], Javier Martínez-Monzó [a], Marta Igual [a], Purificación García-Segovia [a], Rossella Caporizzi [b], Min Zhang [c], Carla Severini [b]

[a] I-FOOD, Instituto Universitario de Ingeniería de Alimentos-FoodUPV, Universitat Politècnica de València, Spain
[b] Department of Agriculture, Food, Natural Resources and Engineering, University of Foggia, Italy
[c] State Key Laboratory of Food Science and Technology, Jiangnan University, Wuxi, China

ARTICLE INFO

Keywords:
3D food printing
Virtual instrument
Consumer co-creation
Fused deposition modelling
Gummies
Delivery systems

ABSTRACT

This paper explores the co-design and development of customizable 3D printed gummies as delivery systems for micronutrients. A virtual instrument, VI, enabling the consumers to select the main morphological properties and to indicate their own requirements of micronutrients was designed and developed. Such digital information was utilised to design gummies containing a void space to be filled with customised amounts of micronutrients. The starch-agar gel used for the printing experiments carried out at 50 °C through a narrow nozzle of 0.4 mm, showed a good printability performance obtaining a precise replica of the digital model. However, slight printing inaccuracies were observed through 2D/3D microtomographic images due to an improper solidification of the ink-gel during the closing movements of the voids. The 3D-printed gummies were described for the main texture properties showing low hardness (<6.87N), cohesiveness, and springiness which changed as a function of time.

1. Introduction

Malnutrition is a global problem. Deficient food intake, poor dietary quality, and limited nutrients bioavailability, greatly contribute to various pathologies (Ramakrishnan, 2002). Among these, deficiencies in micronutrients - i.e. vitamins and minerals - can cause threats to the quality of life (WHO, 2024).

One-third of the population suffers from at least one form of micronutrient deficiency with negative health effects (Han et al., 2022). For instance, iron deficiency is humans' most prevalent nutritional problem affecting more than 2 billion persons (Gardner et al., 2023; Arevalo et al., 2018; Ramakrishnan, 2002; Marley and Brookes, 2023; Tang and Sholzberg, 2024; Latham, 2002).

3D Printing is a widely utilised technology in many sectors of manufacturing (Berman, 2012; Paxton et al., 2024) due to its unique capability of converting a digital model into a physical object. This opens many potentialities such as market innovation, the creation of customised products, and the transition toward an on-demand manufacturing system, among others (Ling et al., 2022; Waseem et al., 2023) offering positive social, economic, and environmental impacts contributing to the sustainable development goals (ONU, 2015; Wang et al., 2023).

The emerging world of 3D Food Printing, 3DFP, is one of the most recent and interesting innovations in the food sector. Through 3DFP, one can digitally design a 3D model and use such digital information to build a tangible/edible structure through the precise control of the printing movements and the deposition of the ink food. 3DFP widely extends the field of food manufacturing (Nachal et al., 2019; Sandhu and Singh, 2022) enabling the creation of sensorial and nutritionally customized food products, the production of inhomogeneous food shapes and internal structures, food waste reduction and on-demand food manufacturing (Eswaran et al., 2023; Nachal et al., 2019; Sehgal et al., 2022; Derossi et al., 2024). A large body of scientific papers have been dedicated to the rheological properties of the food ink (Barrios-Rodríguez et al., 2024; Kim et al., 2017; Matas et al., 2023; Nijdam et al., 2021; Severini et al., 2016; Kadival et al., 2023; Thangalakshmi et al., 2021, 2022; Liu et al., 2019) as well as to the setting of the 3D printing parameters and their effect on the quality of 3D-printed food (Godoi et al., 2019; Lee, 2021; Varvara et al., 2021; Souza et al., 2024).

In addition, several food materials have been tested for 3D food printing such as gels (García-Segovia et al., 2020; Nijdam et al., 2022;

* Corresponding author. Via Napoli 25, 71122, Foggia, Italy.
E-mail address: antonio.derossi@unifg.it (A. Derossi).

https://doi.org/10.1016/j.jfoodeng.2024.112371
Received 1 June 2024; Received in revised form 16 October 2024; Accepted 22 October 2024
Available online 22 October 2024

Rahman et al., 2020a) also added with fruit pulp (Molina-Montero et al., 2023), cereal snacks (Derossi et al., 2020; Uribe-Wandurraga et al., 2020), fruits and vegetables (Fan et al., 2020; Ricci et al., 2018), gluten-free dough (Matas et al., 2022), etc. (Martínez-Monzó et al., 2019; Huang et al., 2023; Mantihal et al., 2019; Nijdam et al., 2022 Anukiruthika et al., 2020; Chakraborty et al., 2023; Chen et al., 2022; Lipton et al., 2010; Wang et al., 2018; Godoi et al., 2016)). Furthermore, gelling agents (Rahman et al., 2020b; Sharma et al., 2024; Zhang et al., 2022) and new ingredients have been studied to improve the printability performances of the ink food opening new perspective in term of the precision in depositing nutrients/ingredients and for high accuracy in printing.

For instance, oleogel consisting of vegetable oil and beeswax has been used to create a highly printable material (Shi et al., 2021) and more complex systems such as hybrid gelator inks of beeswax-carrageenan-xanthan (Tian et al., 2022). Bigels consisting of aqueous and lipid phases gelled utilising hydro- and organogelators have shown excellent rheological properties and the ability to include and protect lipophilic and hydrophilic nutrients and bioactive (Fernandes et al., 2023).

Despite the extensive body of literature on 3DFP, few papers have delved into the area of nutritionally customized 3D-printed food products. Most existing papers utilised a straightforward approach consisting in the mixing of several ingredients with pre-defined ratios, to ensure nutritional contents able to fit the requirements of different consumer groups (Derossi et al., 2018). While this is a interesting strategy, it shows several engineering and practical problems, such as: a) the necessity of dedicated mixing system upstream of the deposition; b) the difficulty of mixing small amounts of ingredients, especially micronutrients; c) the need of providing constantly rheological properties to ensure the food formula can be easily printed. Given this, novel strategies would be of great usefulness for the practical implementation of 3DFP in the field of the customised food industry.

Based on these considerations, this paper proposes a novel technological strategy for developing 3D-printed gummies capable of accommodating customized doses of micronutrients. A virtual instrument (VI) was developed to engage consumers in the co-creation of gummies tailored to their preferred morphological characteristics and individual micronutrient requirements. These information were used to digitally design and fabricate 3D-printed gummies with internal voids designed to hold customized micronutrient doses. The 3D printing experiments employed a highly printable starch-agar ink-gel, ensuring high quality of the 3D printed gummies.

2. Materials and methods

2.1. Ink-gels preparation

Ink-gels were prepared by using a starch refined from waxy maize 'Ultratex' (Ultratex, special Ingredients), and agar-agar (Special Ingredients, EU). The gels were separately prepared by using the above ingredients. Ultratex powder (7% w/w) was dissolved in water at room temperature by continuously stirring the solution till the gel was obtained. Then the gel was passed through a strainer (400 μm) to separate eventual lumps ensuring its homogeneity and maintained at 50 °C. Agar-agar (6% w/w) was dissolved in water and heated at 95 °C for 10 min and then cooled at 50 °C. Finally, the two gels were mixed in the ratio of 50/50 for 2 min to ensure a homogeneous distribution, obtaining ink-gel then distributing into 50 mL syringes maintained at 50 °C till 3D printing experiments.

2.2. Rheological properties of the ink-gel

Rheostress 1 rheometer (Thermo Haake, Karlsruhe, Alemania) was used to characterise the printing material. A 0–150 Hz frequency flow curve test was performed to obtain the power law index (n) and consistency index (k). Then, the linear viscoelastic region (LVR) was studied at 1 Hz from 0,1 Pa–10 Pa. Finally, the oscillatory test was carried out with a stainless-steel plate-plate of 60 mm of diameter, 1 mm gap, 1 Pa and frequency from 0.1 to 10 Hz. Viscous modulus (G''), elastic modulus (G'), complex modulus (G^*), tan δ (G''/G'), and apparent viscosity (η^*) parameters were obtained. All tests were measured at 50 °C in triplicate.

2.3. Digital models and virtual instrument

2.3.1. Virtual instruments for the co-creation of customized 3D digital models for 3D printing applications

The 3D digital models utilised for printing the gummies consist of a cube 20x20 × 8 mm and internal voids of different shapes, dimensions, and locations. While the dimension of such voids is estimated based on the individual requirements of the micronutrients, the geometrical shape can be selected by the user. This adds another co-creation dimension which can enhance the consumer's acceptance considering the overall effect of the visual aspect on the sensory perception (Lin et al., 2020; Pereira et al., 2021). With this aim a virtual instrument, VI, was developed by using LabVIEW (National Instrument, https://www.ni.com/en.html).

2.3.2. Slicing the 3D digital models and setting printing conditions

The 3D digital models were printed by using the following conditions: layer height of 0.33 mm, initial layer height being 0.27 mm, nozzle diameter 0.4 mm; printing speed 30 mm/s; printing speed of the infill 25 mm/s, printing temperature of 50 °C; travel speed of 70 mm/s; retraction distance of 4.0 mm; flow of 4.0%. Under these conditions, a total of 24 layers were deposited during the printing process. Foodbot 3D chocolate Printer (Changxing Shiyin Technology Co., Zhejiang, China) was used for the printing experiments. To fill the voids, the printing process was programmed to stop for 10 s and 20 s before restarting for printing the remaining layers.

2.4. Assessment of the printing fidelity

After printing, the samples were analysed for their main morphological properties and compared with the digital models aiming to assess the printing fidelity. Photographic images of the samples were acquired and analysed by using ImageJ software (ImageJ, NIH, Washington, DC, USA) after proper scale calibration. The width, height, and length of the samples were measured after the printing and every 60 min of storage at room temperature for a total of 6 h to evaluate potential shape changes during a range of time (i.e. swelling) we deliberately considered sufficient for daily consumption.

2.5. X-ray micro CT 2D/3D images

2D/3D X-ray microtomographic images were acquired by using a Skyscan 1174 X-ray (Skyscan, Belgium). The following scanning conditions have been utilised: resolution of 28.5 μm; step angle of 0.2° on a total of 180°, exposure time 1200 ms, 50 kV; averaging frame of 3; total scanning time of 54 min. Image reconstruction was performed by using Nrecon 1.6.2.0 software (Bruker, Belgium). Initially, a region of interest, ROI, representing all the samples has been defined. Then, binary images were created by using a segmentation approach: first, the histogram of the grey-scale image was studied to individuate initial lower and upper threshold values. Then, such values were used as input data to perform the binarization by using the function 'global thresholding' by CTAn 1.12.0.0. (Bruker, Belgium).

2.6. Texture profile analysis (TPA)

A TPA test was carried out to describe the textural properties of the 3D-printed samples. Double compression tests were performed by using

a TA.XT.plus texturometer (Stable Micro Systems, Godalming, Surrey, UK) equipped with a plate 45 mm diameter in the following conditions: compression force with a load cell of 50 kg, trigger force of 20 g; pre-test speed of 10 mm/s; the test speed of 1 mm/s; the post-test speed of 5 mm/s; deformation of 75%. Hardness, adhesiveness, springiness, cohesiveness, and gumminess - as defined by Ji et al. (2022) and De Avila et al. (2014) - were analysed to describe the main texture properties of the 3D printed gummies.

3. Result and discussion

3.1. Development of a 3D digital model based on individual preferences and micronutrient requirements

Fig. 1 shows the front panel on which anyone can introduce their micronutrient requirements (μg) utilised as input data for generating the digital models. In addition, it enables to select the shape of the internal void according to the principle of multisensory integration and cross-modal correspondences defining the importance of the association between visual attributes - i.e. geometry and colour - and other sensory perceptions that can drive the consumer's acceptances (Chuquichambi et al., 2024; Corradi et al., 2020). According to such principles, five selectable void shapes have been designed: two cylinders (TC), a diagonal cylinder (DC), two triangles (TT), one sphere (OS), and two spheres (TS). Furthermore, the front panel of Fig. 1 shows some additional information: 1. the estimated volume of the void phase required to accommodate the desired amount of micronutrients; 2. the estimated dimension (e.g. radius) of the void shapes; 3. the digital model of the obtained gummy to be used for the 3D printing experiments.

Fig. 2 shows the block diagram consisting in the graphical code representing how the digital information flows through the objects of the front panel. The block diagram contains the functions and the node enabling it to convert the input data in the customised digital model. As representative examples, we considered the vegan people and an overall daily requirement for vitamin B12 of 2.4 μm/d. In addition, the use of a standard solution of vitamin B12 with a concentration of 50 μg/mL, and a length of the internal cylindrical voids of 18 mm were used as input data. However, other dimensions and concentrations could be utilised extending the application to various digital models.

Given this, after any user could indicate his requirements in micronutrients, the virtual instrument would compute the volume of the micronutrient solution at a fixed concentration and then, the corresponding void space would be designed in the digital model of the gummy. Finally, such a model can be used to build the customised gummies by depositing the ink-gel and filling the void space with a precise quantity of micronutrients. Fig. 3 shows examples of the 3D digital models, their schematic representation, and the related morphological dimensions. The designed models are characterised by internal volumes of 0.12 mL, 0.21 mL, 0.065 mL, 0.028 mL, and 0.09 mL respectively for DC, TC, OS, TS and TT.

3.2. Rheological properties of the ink-gels

At first, the rheological properties of the gel were analysed. The gel prepared at 50 °C was characterised using a flow curve, and the data is collected in Fig. 4. The higher the frequency, the lower the stress to be applied and the lower the viscosity of the fluid. Therefore, ink-gel presents a pseudoplastic behaviour at 50 °C. Law index (n) was 0.5187, between 0 and 1; this confirms pseudoplastic behaviour again, and the consistency index (k) was 17.465 $Pa*s^{(0.5187)}$. Similar (±2) values of consistency index were observed on mango pulp with 25 °Brix at 30 °C (Ortega Quintana et al., 2015), commercial salad dressing (Lady's Choice MayoLite) with 0 days stored at 4 or 30 °C (Mohamad et al., 2019), orange juice with 65.1 % of solids and tomato juice with 18.7 % of solid content at 40.7 °C (Krokida et al., 2001). On the other hand, the linear viscoelastic region (LVR) test showed that the region from 0.1 to 10 Pa is part of the LVR, the inflection point was not observed. The data obtained at 1 Hz from the oscillatory test found that the parameters of the elastic modulus and complex modulus were similar (G′-G*), being 96 and 106 Pa, respectively. The offset angle (δ) was 24.4°, which is under 45°. These both aspects explain a predominant elastic behaviour.

3.3. Morphological and microstructure properties of the 3D printed sample

Although there is a large body of scientific documents analyzing the accuracy of the 3D printing of edible gels (Ahmadzadeh and Ubeyitogullari, 2023; Cheng et al., 2024; Feng et al., 2024; Yu et al., 2022), to

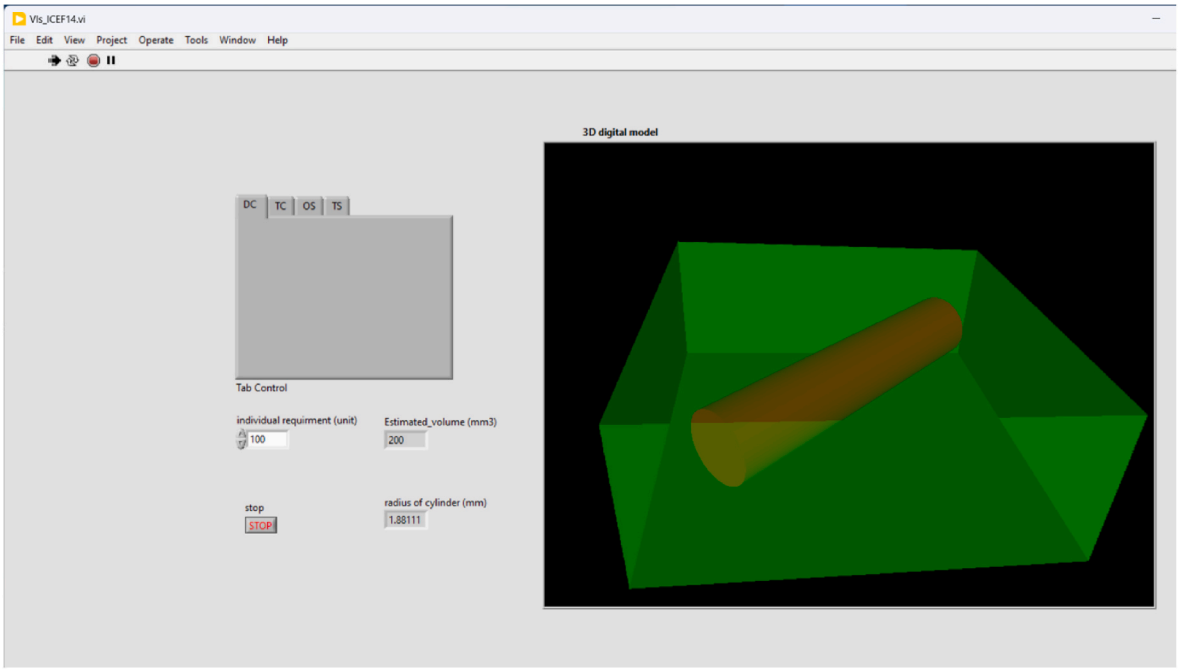

Fig. 1. Representative image of the front panel of virtual instrument, VI, for the on-demand co-creation of 3D digital models.

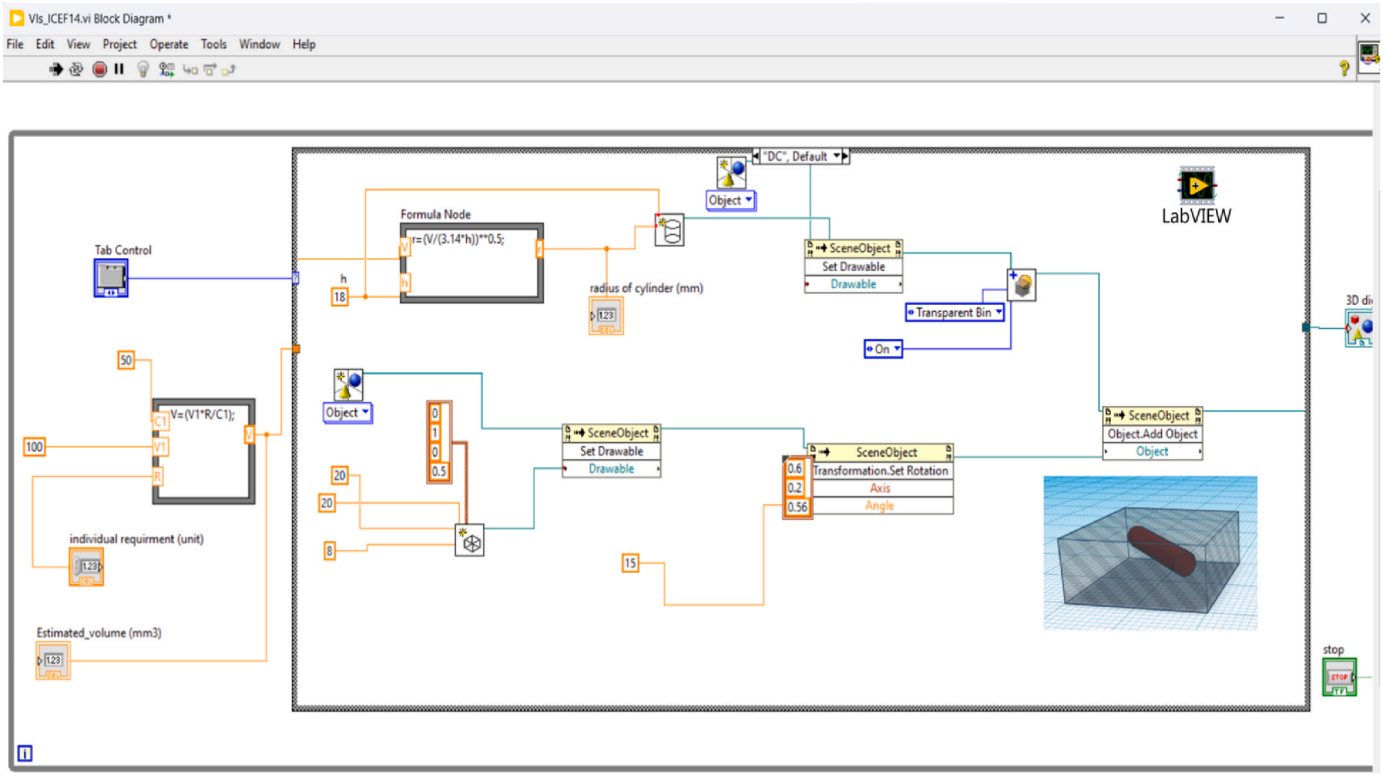

Fig. 2. Example of the block diagram developed for the on-demand co-creation of 3D digital model.

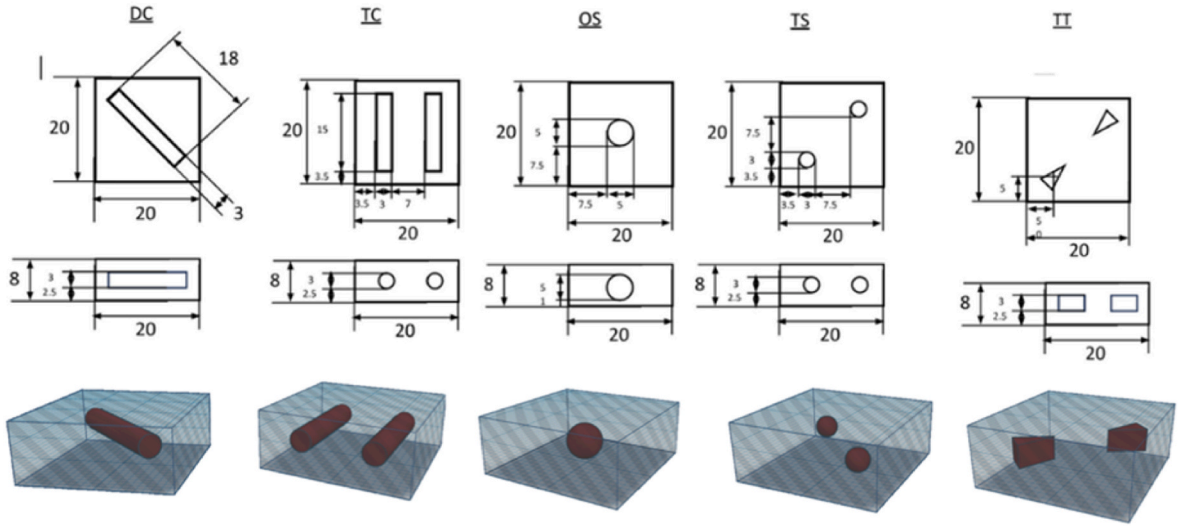

Fig. 3. 3D digital models designed in mm for the 3D printing experiments. a) diagonal cylinder (DC), b) one sphere (OS), c) two cylinders (TC), d) two spheres (TS), e) two triangles (TT).

our knowledge, only a few papers have studied structures with embedded voids in 3D-printed gummy (Fahmy et al., 2022). At first, the weight of the 3D printed samples, always between 3.125 ± 0.104 and 3.252 ± 0.037 highlighted a negligible variability and, therefore, the high precision of the ink-gel deposition (data not shown). Above all, the visual inspection of the printed gummies argues for the quality of the replica of the 3D digital models (as reported in Fig. 5), for both the external and internal morphologies. The details of the sample DC highlight the printing precision of each overlapping layer (DCb) deposited by using a thin nozzle of 0.4 mm and a layer height of 0.33 while figure DCa calls attention to the presence of some air spots on the last few layers before closing the cylindrical void. The latter may be considered minor defects attributed to the difficulty of solidifying the ink-gel when the printing movements initiate closing the cylinder. Indeed, without the adhesion of the liquid ink-gel during material deposition to the previous solid layer, there is a slower cooling and, therefore, a delay in the transition from liquid to solid state. Such conditions induced air spots in the last few layers. Similar results have been obtained for all other samples (Fig. 5). However, such phenomenon is better interpreted and detailed in the section regarding the microstructure properties of the samples.

The printing quality has been quantified by measuring the length in

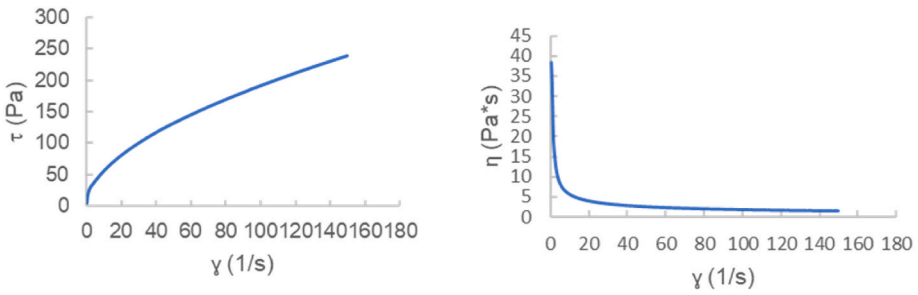

Fig. 4. – Rheological properties of the ink-gel.

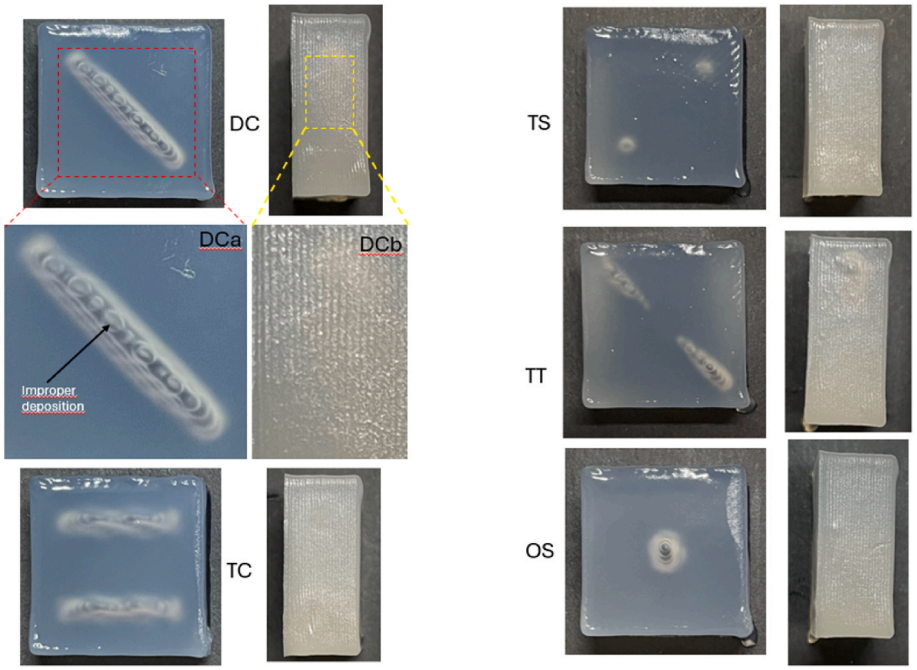

Fig. 5. Photographic images of the 3D printed gummies.

the X-Y plane, the height of the samples (Fig. 6) and their potential changes during storage of 6 h at room temperature. This storage time was deliberately assumed to be enough to envision the opportunity of buying customized 3D-printed gummies from a 3D-print vending machine and consuming such gummies on the same day. Therefore, the data of Fig. 6 provide information about the potential shape changes of the gummies before consumption. Overall, printed samples demonstrate a good fidelity of printing. The length of the gummies was between 18.42 ± 0.02 mm and 20.36 ± 0.05 mm, corresponding to a fractional variation in the range of 1.76%–8%. Similarly, the height of the 3D printed gummies was between 7.63 ± 0.01 mm and 8.73 ± 0.02 corresponding to a fractional variation between 4.5% and 9.2%. Moreover, any significant difference ($p < 0.05$) of sample dimensions along 6 h at room temperature was not observed. These results proved that: 1. The

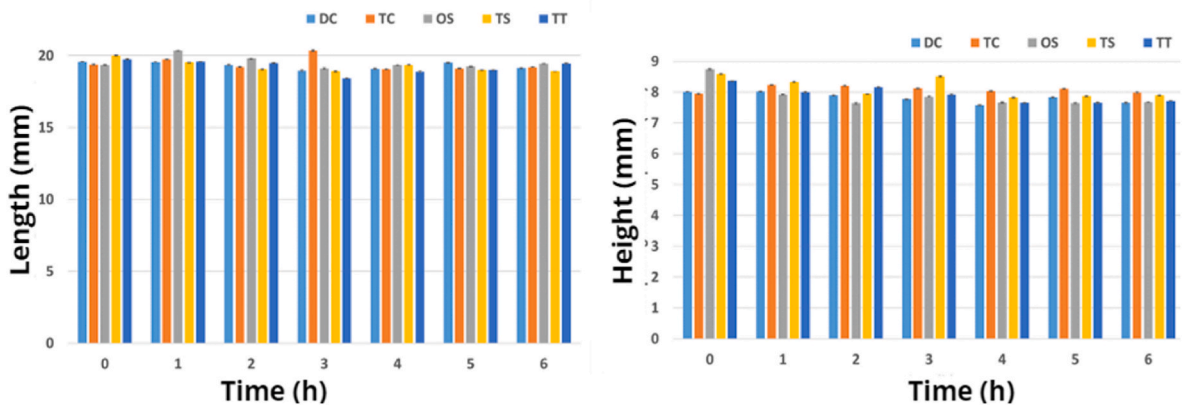

Fig. 6. Main morphological dimensions of the 3D printed gummies. a) length in XY axes; b) height.

obtained starch-agar ink-gel can be used to precisely print objects even when using a thin nozzle of 0.4 mm; 2. 3D printed gummies showed high structural stability.

However, the X-ray images provide more precise information regarding the printing fidelity, while also revealing the microstructural characteristics. Examples of 2D X-ray images of the samples, along with the separated void and solid phases, are shown in Fig. 7. Additionally, the porosity fraction of the samples as a function of their height is presented in Fig. 8.

For sample DC, TC, OS and TS, the bell-shaped curves result from the change of the diameters of the cylindrical and spherical voids as a function of the height of the samples. Therefore, the curve peaks have been compared with the porosity of the digital models shown in Fig. 3. For samples DC and TC, the measured porosity fractions of 13.13% and 19.39% closely matched the digital models, which were of 13.5% and 22.5%, respectively. However, such minor differences may be attributed to the aforementioned improper solidification of the ink-gel during the printing movements. Fig. 9 shows the X-ray images of the cylindrical voids, with detailes on on the topof the samples. Considering a range of 55 slices - from 365 to 420 - and the image resolution of 22.2 μm, the figure shows how the printing process proceeded in the last 1.2 mm (i.e. about 4 layers of printing from the top of the samples). In particular, it is worth noting that slice n.365 represents the last slice before the printing initiates closing the cylindrical void. Given this, although the closing printing movements are expected to generate a sudden increase in density, some regions at low or medium density were observed on the slice n.400. Such a region corresponds to the existence of small air spots and only partially closed regions. With the advancement of the printing process - slice n.410, n.415 and n.420 - only a few air spots were observed. Such images corroborate the hypothesis of the improper ink-gel solidification and the related creation of air spots in the gel, as previously reported in Fig. 5DCa. Finally, the slice n. 420 shows the higher density indicating the absence of air spots.

In the case of OS and TS the peaks of the porosity curve were 4.3% and 1.8% instead of 4.9% and 3.5%, of the 3D digital models, respectively. While in the case of OS, the printed sample sufficiently resembled the digital model, significant divergences were obtained for samples TS (Table 1). This discrepancy was caused by the difference between the designed diameter of the digital model (3 mm) and the actual diameter of the 3D-printed gummies (1.95 mm), indicating a reduction of 35% (Table 1). The result focuses on the inability to accurately replicate voids with a diameter <3 mm in the printing conditions used in these experiments. In addition, the aforementioned lack of solidified gel when the printing movements initiate closing the designed void, reduced the quality of the 3D printed samples. Such issues negatively impacted the overall volume of the internal voids, which were lower than the designed volumes. For instance, in the case of samples DC internal volumes ranging between 0.110 mL and 0.118 mL were measured rather than expected values of 0.120 mL of the digital model. The greater discrepancies were measured for the samples TS with a measured average volume of 0.005 mL in comparison to 0.028 mL of the designed model. On the other hand, a smaller variation was observed for the sample TC with a measured volume of 0.160–0.168 mL in comparison to 0.21 mL of the designed model. Again, the delay in the solidification of the ink-gel during the closing movement of the voids generated a partial drip of the ink inside the voids with the corresponding reduction of the total volume. Further printing experiments performed with a nozzle diameter <0.4 mm, could significantly increase the quality of the samples considering the faster solidification of a thinner filament of the ink-gel.

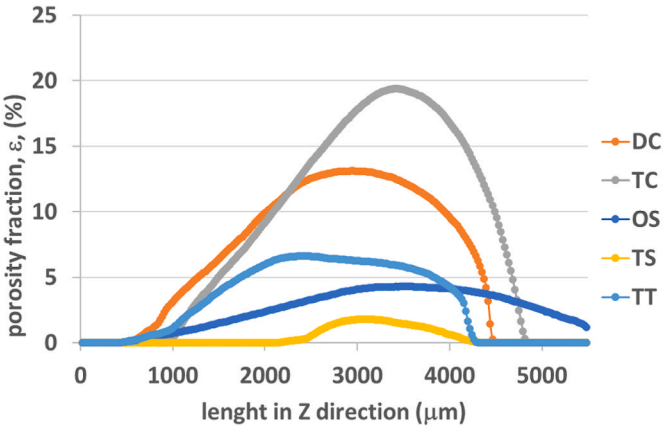

Fig. 8. Total porosity fraction of the 3D printed gummies as a function of the height of samples.

3.4. Textural properties of the 3D-printed gummies

Fig. 10 shows the texture profile of the DC samples during two compression-decompression cycles (i.e. two bites). At first, the behaviour of the samples shows a high repeatability indicating the homogeneity of the ink-gel and the printing process.

During the first compression, two peaks corresponding to the fracturability and the hardness were observed with force values respectively

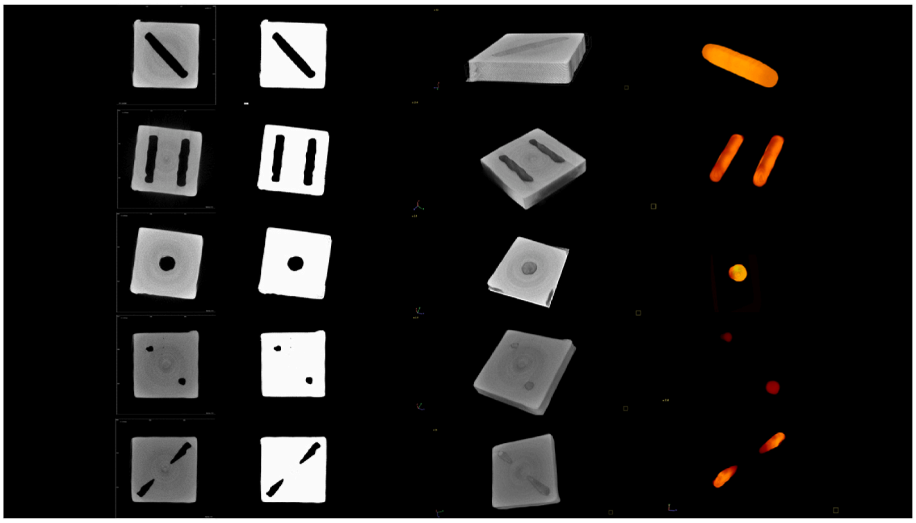

Fig. 7. X-ray images of the 3D printed gummies. a) 2D grayscale image; b) 2D binary images; c) 3D model of the solid phase; d) 3D model of the void phase.

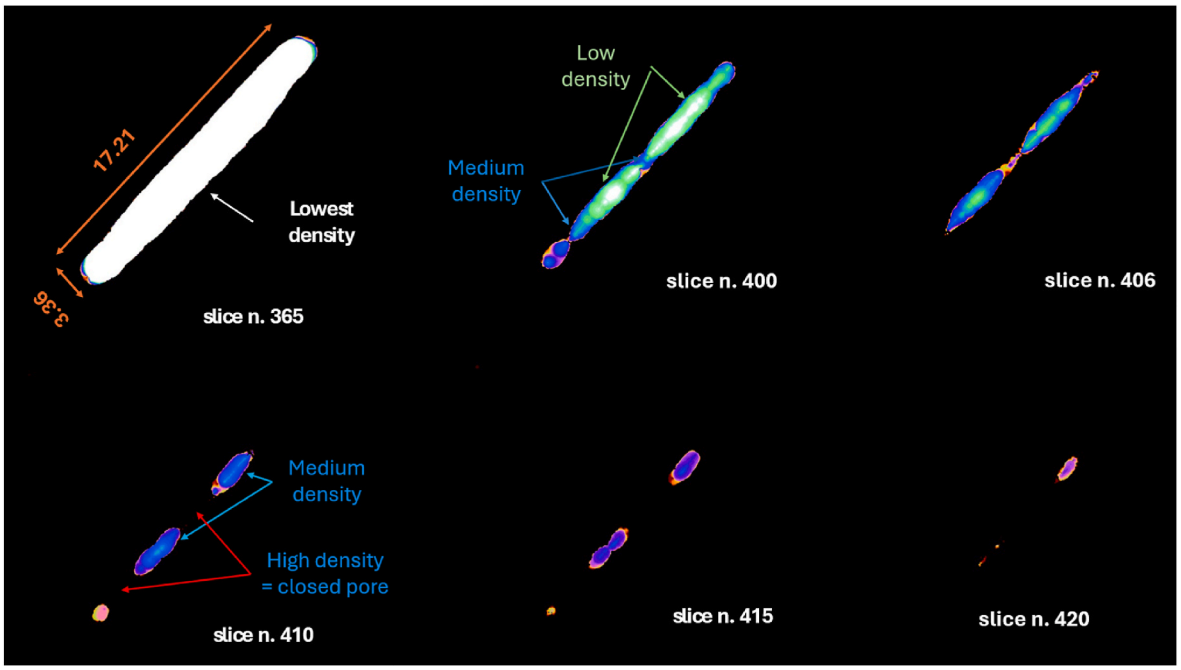

Figs. 9. 2D X-ray microstructure images of the cylindrical voids of DC sample. Coloured maps represent regions at different density values.

Table 1
Morphological properties of the different voids included in the 3D printed gummies. A comparison between the designed models and the printed samples.

	DC		TC		OS	TS	TT	
	Major axis (mm)	Minor axis (mm)	Major axis (mm)	Minor axis (mm)	Diameter (mm)	Diameter (mm)	Height (mm)	Length (mm)
Digital model	18	3	15	3	5	3	2.97	5.06
Experimental	17.21 ± 0.4	3.31 ± 0.2	13.99 ± 0.34	2.67 ± 0.25	4.45 ± 0.22	1.95 ± 0.21	1.92 ± 0.32	7.42 ± 0.41

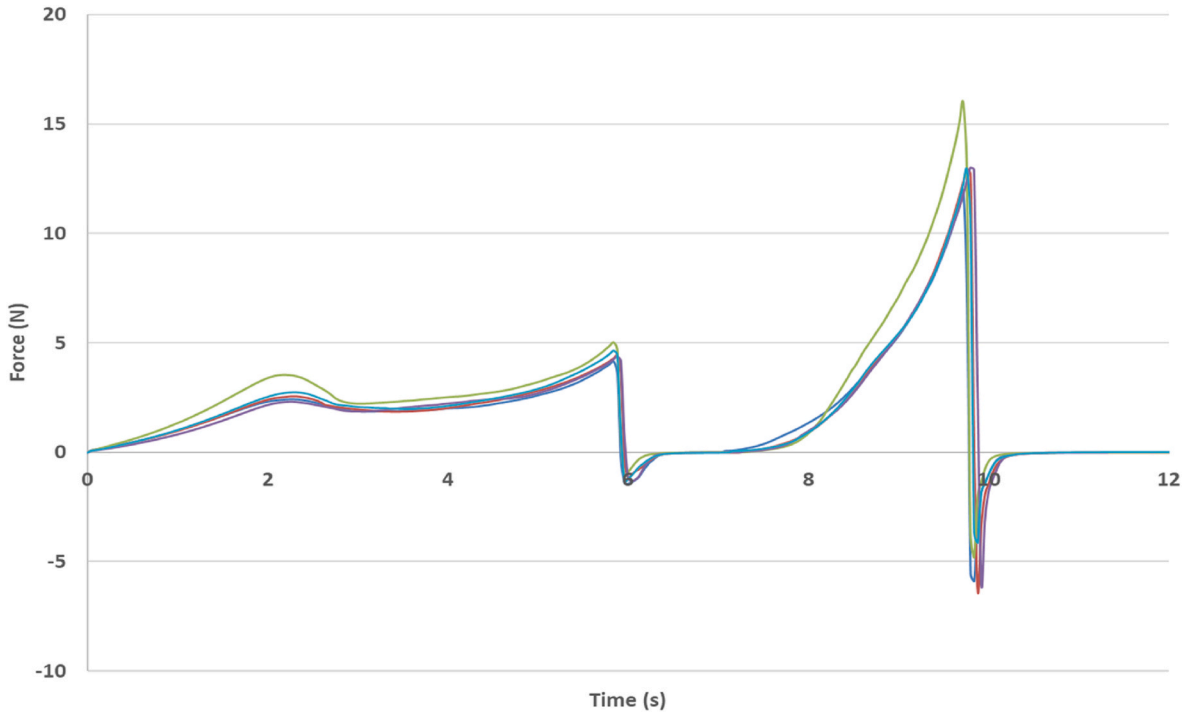

Fig. 10. Texture profile curves of 3D printed gummies, DC, submitted to two compression tests.

of 2.71 ± 0.48 N and 4.51 ± 0.32 N. The hardness indicates the force required to reach a certain level of deformation/penetration. Overall, the hardness was higher than the recent 3D-printed printed ink-gels prepared by using starches and other structuring agents. Ji et al. (2022) by analysing the effect of starch molecular structure on texture properties of 3D printed cubes (infill of 100%) reported values of 1.09, 0.57, 1.21, 0.63, 1.8 and 1.55 N respectively for cassava, wheat, corn, sweet potato, potato, and buckwheat starches. Wedamulla et al. (2023) by studying the printability and the texture properties of 3D printed samples of potato starch-pectin gel, measured texture of about 0.49 N for control samples without pectin. Qiu et al. (2024) measured values in the range of 0.29–0.69 N for 3D printed food formula designed for the elderly and consisting of flaxseed gum and mung bean protein in different proportions. This higher hardness of our samples was the result of the contribution of agar-agar. Other authors (Carranza et al., 2023) printed food formulas prepared by mixing soy protein isolate, SPI, and red cabbage, RC. The authors found a higher range of hardness - between 0.15 and 15.33 N - with the maximum values obtained for the samples obtained by mixing 12.5 g of SPI with 20% wt of Gly and 20–30% of RD. Furthermore (Chao et al., 2023), measured hardness of 0.541 N/cm^2 by analysing 3D printed gels containing chickpea protein isolate and mealworm protein isolate.

The slight negative area observed during the first compression describes the adhesiveness of the gummies that is related to the adhesive force between food and teeth. An average value of −0.286 ± 0.087 N s was observed. This is significantly lower than the data obtained by (Qiu et al., 2024) who studied the texture properties of 3D-printed food prepared for the elderly. In addition, the data were lower than the limit of adhesiveness for food easy-to-swallowing (Kong et al., 2023). Cohesiveness indicates how strong the internal forces of the food are, preventing the fractionating in small particles during chewing and swallowing (Mirazimi et al., 2022). An average value of 0.866 ± 0.034 was observed according to the 3D printed gummy prepared by (Zhou et al., 2023) who mixed peach gum polysaccharides and gelatine in different conditions (0.81–0.97). Such evaluations identify the samples as appropriate for safe swallowing according to the definition of the Ministry of Health, Labour, and Welfare of Japan (Pure et al., 2021).

Fig. 11 shows the average values of texture indices for all 3D-printed gummies. Hardness significantly increased ($p > 0.05$) for DC, TC and OS with values respectively of 4.52 ± 0.33 N, 5.53 ± 6.87 and 6.87 ± 0.40. Considering the sample OS, the higher hardness could be attributable to the lower porosity fraction (i.e. the high relative density) according to the principle of the mechanics of cellular materials for 3D cellular materials as described by Gibson et al. (1982); 1982b. In fact, the diameter of the spherical void of the 3D printed samples - 4.45 mm - led to a porosity <1.44% which is significantly lower than the samples DC and TC with values respectively of 4.62% and 4.89%. Furthermore, considering the sample DC and TC, although the porosity values were similar, the higher hardness for TC could be given by the result of the different internal morphological properties such as the number and the size of the pores and their location in the gummies which modify the thickness of the solid phase (Zhagal et al., 2002; Derossi et al., 2020). Samples TS and TT with porosity fractions of 0.24 and 1.33 % did not show any significant difference of their hardness. Regarding the adhesiveness, the samples did not show any difference, with overall values ranging between −0.154 and −0.396 indicating a negligible adhesive force between food and teeth and, therefore, the ease of swallowing. In general, to facilitate the swallowing a lower degree of adhesion is preferable to avoid a sticky gummy (Wang and Hartel, 2021). The cohesiveness values were between 0.696 ± 0.125 and 1.034 ± 0.041, respectively for samples TT and TC. The highest value of TC informed on the resistance of the sample to deformation and the greater internal forces preventing disintegration in small particles. As for the springiness, the samples showed a recovery of the initial height in the second cycle of 40–50%. Since gumminess and chewiness are calculated from the hardness values (gumminess = hardness × cohesiveness; chewiness = gumminess × springiness), they reflect the previous data, with TC and OS showing the highest values ($p < 0.05$). The gumminess presented by the samples is low, comparable to soy protein-based masses (Carranza et al., 2023) and slightly higher than gels prepared from legumes (Lee and Hong, 2023).

To better describe the potential change of the texture properties along the 6 h of storage, a PCA was performed by including the storage time as input variables. The plot of the loading for all 3D printed samples is reported in Fig. 12. While 82% of the total variance of the samples was explained by three principal components, the loading plot of the first two PCs (Fig. 12) enables us to describe 70% of the variance (i.e. 44.42% and 24.59 for PC1 and PC2 respectively). On PC1, the higher contribution were given by gumminess (0.260), cohesiveness (0.198) and

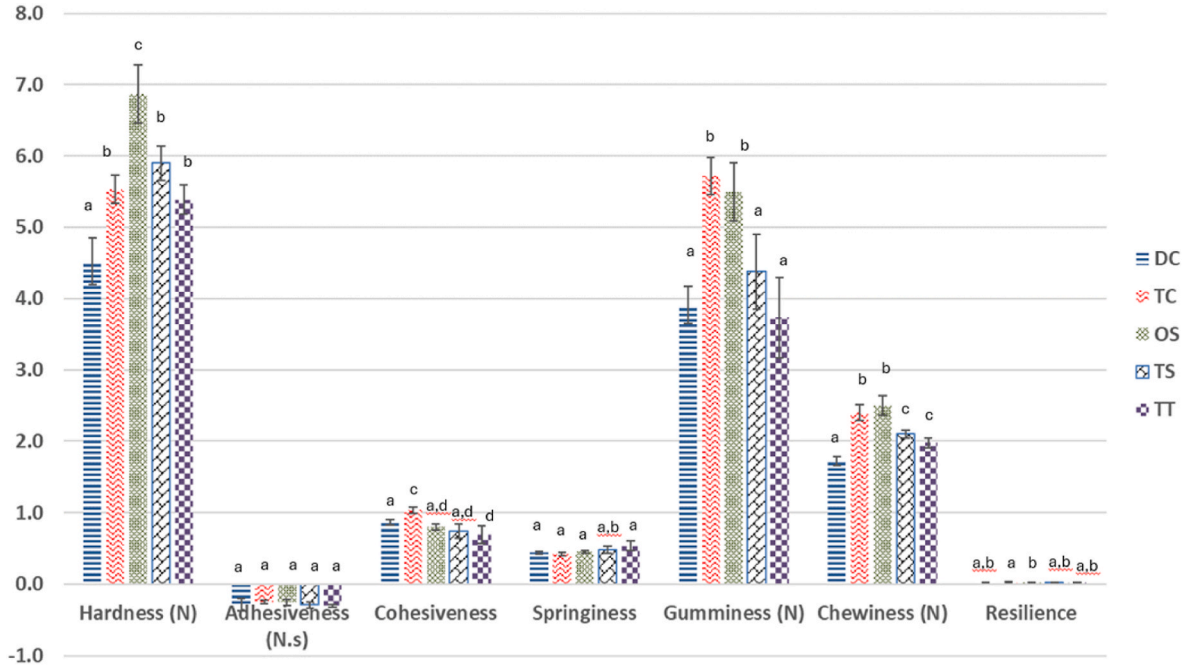

Fig. 11. Texture properties of the 3D printed gummies.

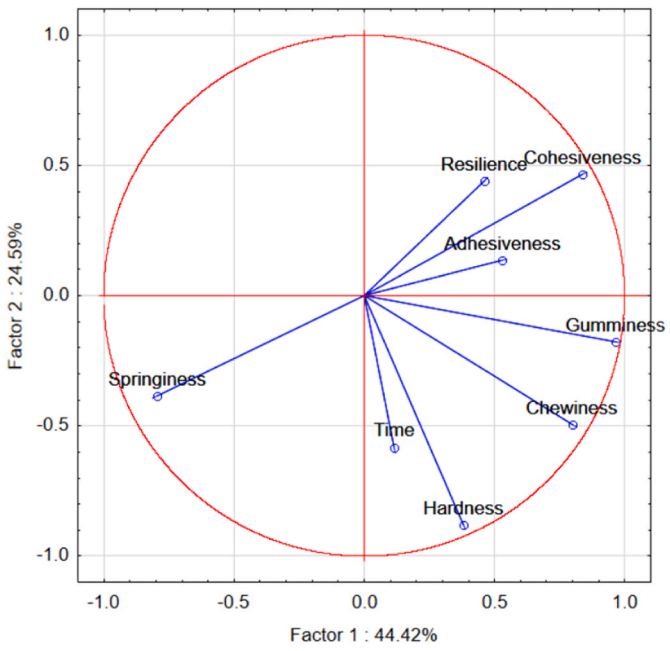

Fig. 12. PCA loading plot of the 3D printed samples storage time by using the change of texture parameter as a function of storage time.

springiness (0.177). Differently, on the PC2 the hardness and the storage time showed the highest contribution (i.e. 0.394 and 0.172) in explaining the variance of the experimental data. The springiness was negatively related to all other texture properties being the only variable in the negative part of the PC1. As expected, the gumminess and chewiness are located very close to the hardness, being the first two properties computed through the data of hardness. In addition, such properties, especially the hardness, fall close to the variable time indicating that the force required to deform the samples increased with storage time. This would be explained by considering starch retrogradation which can generate a denser molecular organisation of amylose and amylopectin and, therefore, an increase of the hardness of the samples (Jiang et al., 2020). Similar results have been reported by Wedamulla et al. (2023) who studied the printability and the post-printing behaviour of ink-gel prepared by mixing starch and pectin. As a result of starch retrogradation, the samples were categorised as a function of the storage time and texture properties ($p < 0.05$). A representative example of the score plot for the samples DC is reported in Fig. 13. DC samples were well discriminated in three different groups defining the storage time - 0h, 3h and 6h - and along the direction of the variables time, hardness, chewiness and gumminess. More specifically, the samples showed a significant increase ($p < 0.05$) of the hardness after 3h of storage while any significant increase was not observed after 6 h. Similar results were observed for the other 3D printed samples confirming the increase of hardness as a function of time (data not shown).

Finally, the photographic images of the 3D printed DT over 6 h of storage at room temperature are shown in Fig. 14. Although the main morphological dimensions were constant along storage (Fig. 6), the external appearance shows some changes probably resulting from the starch retrogradation as previously discussed. Any change in the weight of samples was not observed (data not shown). Further experiments are needed to explore the best storage conditions.

4. Conclusion

A novel strategy for developing 3D-printed gummies capable of accommodating customizable amounts of micronutrients has been proposed. A virtual instrument was developed to engage consumers in the design process and to indicate their specific micronutrient requirements. This digital information was used to create a 3D model containing voids of precise volume embedded in the 3D-printed gummies. A starch-agar ink-gel was utilised in the printing experiments with a thin nozzle of

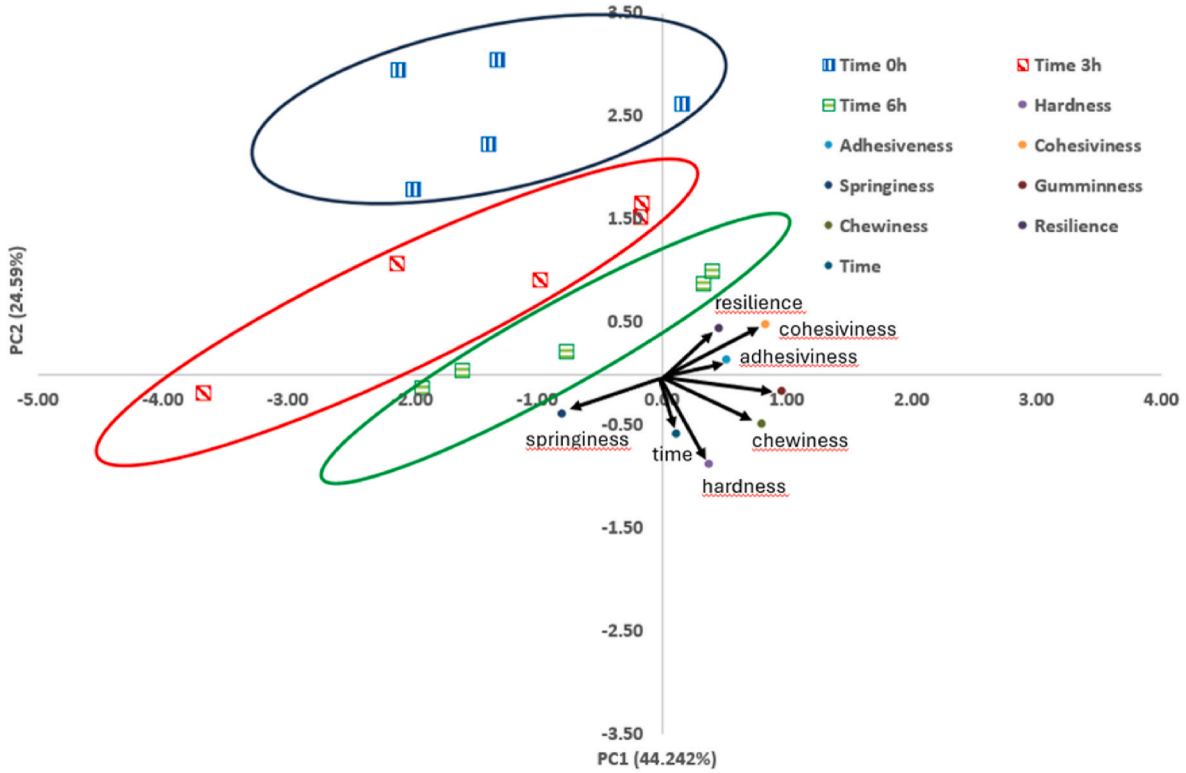

Fig. 13. Score plot in the PC1-PC2 space of the 3D printed samples DC obtained analyzing the change of texture properties as a function of storage time.

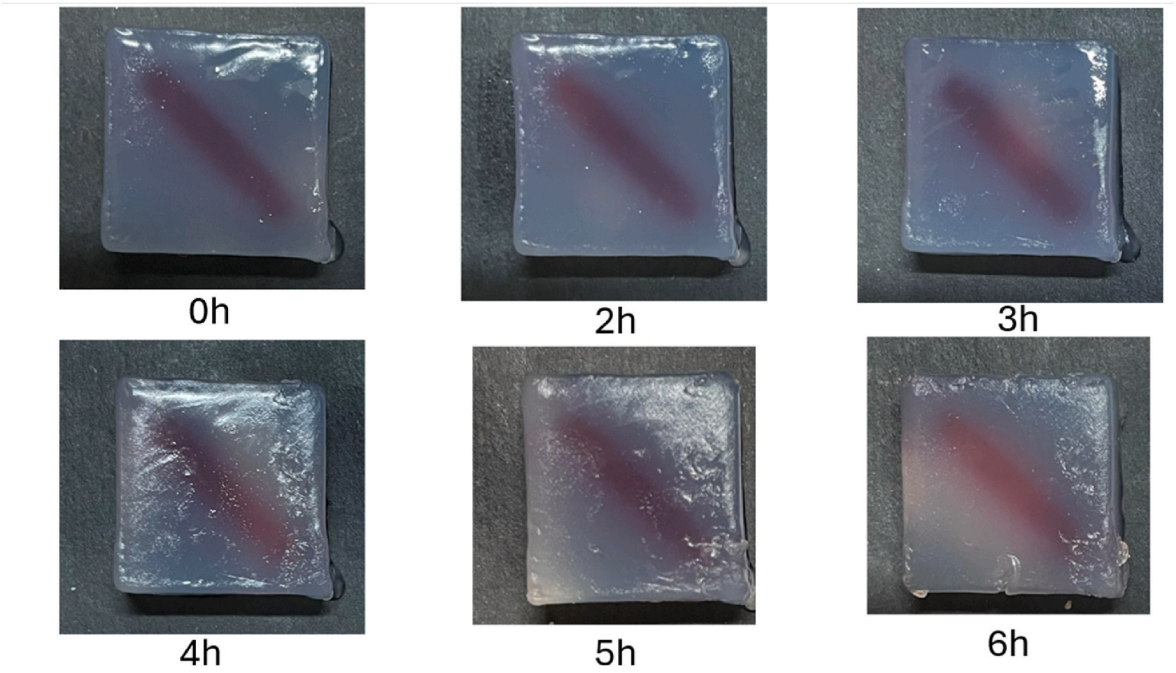

Fig. 14. Photographic images of the DC samples filled with red colourant over storage time of 6 h at room temperature.

0.4 mm. This ink-gel exhibited good flowability at 50 °C and a rapid transition from liquid to solid, ensuring appropriate structural stability and a precise replica of the 3D models. However, minor discrepancies between the digital model and the actual volume of the internal voids were observed. These discrepancies were caused by a delay in the solidification of the ink-gel during printing movements, which altered the balance between material deposition and printing movements, leading to the dripping of liquid ink-gel into the voids (resulting in a minor decrease in the designed volume) and the creation of air pockets. Further experiments addressing the challenge of using very thin filaments could help mitigate these issues by facilitating faster cooling and solidification of the ink. In addition, data regarding the assessment of micronutrients after their incorporation in the 3D printed gummies are needed before a practical application of this new strategy. Although additional experiments could significantly improve the final quality of the printed gummies, the proposed strategy reveals innovative opportunities for the practical implementation of customized food manufacturing, where the integration of individual data and 3D food printing can make a positive contribution.

Funding

This research was funded by MCIN/AEI/10.13039/501100011033/ through project PID2020-115973RB-C22 and the FPI PhD contract granted by the Universitat Politècnica de Valencia subprograma 1 (PAID 01 21).

CRediT authorship contribution statement

Adrián Matas-Gil: Writing – review & editing, Writing – original draft, Methodology, Investigation, Formal analysis, Data curation. **Antonio Derossi:** Writing – review & editing, Writing – original draft, Visualization, Supervision, Methodology, Data curation, Conceptualization. **Javier Martínez-Monzó:** Writing – review & editing, Writing – original draft, Supervision. **Marta Igual:** Writing – review & editing. **Purificación García-Segovia:** Writing – review & editing. **Rossella Caporizzi:** Writing – review & editing, Methodology, Investigation, Data curation. **Min Zhang:** Writing – review & editing. **Carla Severini:** Writing – review & editing.

Declaration of competing interest

None.

Data availability

Data will be made available on request.

References

Ahmadzadeh, S., Ubeyitogullari, A., 2023. Enhancing the stability of lutein by loading into dual-layered starch-ethyl cellulose gels using 3D food printing. Addit. Manuf. 69. https://doi.org/10.1016/j.addma.2023.103549.

Anukiruthika, T., Moses, J.A., Anandharamakrishnan, C., 2020. 3D printing of egg yolk and white with rice flour blends. J. Food Eng. 265. https://doi.org/10.1016/j.jfoodeng.2019.109691.

Arevalo, K.J., Tandazo, A.S., Balarezo, S. dl A., Guadalupe, C.L., 2018. Dialnet-MALNUTRICIONEnfermedadDeLosPaisesEnDesarrollo-6732901. Revista Científica Mundo de La Investigación y El Conocimiento 2 (1).

Barrios-Rodríguez, Y.F., Igual, M., Martínez-Monzó, J., García-Segovia, P., 2024. Multivariate evaluation of the printing process on 3D printing of rice protein. Food Res. Int. 176, 113838. https://doi.org/10.1016/j.foodres.2023.113838.

Berman, B., 2012. 3-D printing: the new industrial revolution. Bus. Horiz. 55 (2), 155–162. https://doi.org/10.1016/j.bushor.2011.11.003.

Carranza, T., Guerrero, P., Caba, K. de la, Etxabide, A., 2023. Texture-modified soy protein foods: 3D printing design and red cabbage effect. Food Hydrocolloids 145. https://doi.org/10.1016/j.foodhyd.2023.109141.

Chakraborty, P., Eqbal, M.D., Ahmed, J., 2023. Three-dimensional printing and its application to legume proteins: a review. In: Legume Science, vol. 5. John Wiley and Sons Inc. https://doi.org/10.1002/leg3.172, 2.

Chao, C., Lee, J.H., Kim, I.W., Choi, R.Y., Kim, H.W., Park, H.J., 2023. Investigation of 3D-printable chickpea-mealworm protein mixtures and their bolus rheology: a soft-textured and safe-swallowing food for the elderly. Food Biosci. 54. https://doi.org/10.1016/j.fbio.2023.102924.

Chen, J., Sun, H., Mu, T., Blecker, C., Richel, A., Richard, G., Jacquet, N., Haubruge, E., Goffin, D., 2022. Effect of temperature on rheological, structural, and textural properties of soy protein isolate pastes for 3D food printing. J. Food Eng. 323. https://doi.org/10.1016/j.jfoodeng.2021.110917.

Cheng, Y., Gao, W., Kang, X., Wang, J., Yu, B., Guo, L., Zhao, M., Yuan, C., Cui, B., 2024. Effects of starch–fatty acid complexes with different fatty acid chain lengths and degrees of saturation on the rheological and 3D printing properties of corn starch. Food Chem. 436. https://doi.org/10.1016/j.foodchem.2023.137718.

Chuquichambi, E.G., Munar, E., Spence, C., Velasco, C., 2024. Individual differences in sensitivity to taste-shape crossmodal correspondences. Food Qual. Prefer. 115. https://doi.org/10.1016/j.foodqual.2024.105110.

Corradi, G., Chuquichambi, E.G., Barrada, J.R., Clemente, A., Nadal, M., 2020. A new conception of visual aesthetic sensitivity. Br. J. Psychol. 111 (4), 630–658. https://doi.org/10.1111/bjop.12427.

De Avila, M.D.R, Cambero, M.I., Ordóñez, J.A., De la Hoz, L., Herrero, A.M., 2014. Rheological behaviour of commercial cooked meat products evaluated by tensile test and texture profile analysis (TPA). Meat Sci 2 (98), 310–315. https://doi.org/10.1016/j.meatsci.2014.05.003.

Derossi, A., Caporizzi, R., Azzollini, D., Severini, C., 2018. Application of 3D printing for customized food. A case on the development of a fruit-based snack for children. J. Food Eng. 220, 65–75. https://doi.org/10.1016/j.jfoodeng.2017.05.015.

Derossi, A., Caporizzi, R., Paolillo, M., Severini, C., 2020. Programmable texture properties of cereal-based snack mediated by 3D printing technology. J. Food Eng. 289. https://doi.org/10.1016/j.jfoodeng.2020.110160.

Derossi, A., Spence, C., Corradini, M.G., Jekle, M., Fahmy, A.R., Caporizzi, R., Devahastin, S., Moses, J.A., Le-Bail, A., Zhou, W., Zhang, M., Bhandari, B, Severini, C., 2024. Personalized, digitally designed 3D printed food towards the reshaping of food manufacturing and consumption. npj Sci Food 8, 54. https://doi.org/10.1038/s41538-024-00296-5.

Eswaran, H., Ponnuswamy, R.D., Kannapan, R.P., 2023. Perspective approaches of 3D printed stuffs for personalized nutrition: a comprehensive review. In: Annals of 3D Printed Medicine, vol. 12. Elsevier Inc. https://doi.org/10.1016/j.stlm.2023.100125.

Fahmy, A.R., Vogt, U.T., Jekle, M., Becker, T., 2022. Hardness targeted design and modulation of food textures in the elastic-regime using 3D printing of closed-cell foams in point lattice systems. J. Food Eng. 320. https://doi.org/10.1016/j.jfoodeng.2022.110942.

Fan, H., Zhang, M., Liu, Z., Ye, Y., 2020. Effect of microwave-salt synergetic pre-treatment on the 3D printing performance of SPI-strawberry ink system. LWT 122. https://doi.org/10.1016/j.lwt.2019.109004.

Feng, M., Zhang, M., Mujumdar, A.S., Guo, Z., 2024. Influence of components interaction in recombined food gels on 3D printing: a comprehensive review. In: Food Hydrocolloids, vol. 151. Elsevier B.V. https://doi.org/10.1016/j.foodhyd.2024.109782.

Fernandes, A.S., Neves, B.V., Mazzo, T.M., Longo, E., Jacob-Lopez, E., Zepka, L.Q., de Rosso, V.V., 2023. Bigels as potential inks for extrusion-based 3d food printing: effect of oleogel fraction on physical characterization and printability. Food Hydrocolloids 144. https://doi.org/10.1016/j.foodhyd.2023.108986.

García-Segovia, P., García-Alcaraz, V., Balasch-Parisi, S., Martínez-Monzó, J., 2020. 3D printing of gels based on xanthan/konjac gums. Innovative Food Sci. Emerging Technol. 64. https://doi.org/10.1016/j.ifset.2020.102343.

Gardner, W.M., Razo, C., McHugh, T.A., Hagins, H., Vilchis-Tella, V.M., Hennessy, C., Taylor, H.J., Perumal, N., Fuller, K., Cercy, K.M., Zoeckler, L.Z., Chen, C.S., Lim, S.S., Aravkin, A.Y., Arndt, M.B., Bishai, J.D., Burkart, K., Chung, E., Dai, X., et al., 2023. Prevalence, years lived with disability, and trends in anaemia burden by severity and cause, 1990–2021: findings from the Global Burden of Disease Study 2021. The Lancet Haematology 10 (9), e713–e734. https://doi.org/10.1016/S2352-3026(23)00160-6.

Gibson, L.J., Ashby, M.F., 1982. The mechanics of three-dimensional cellular materials. Proceedings oft he Royal Society A, 382. https://doi.org/10.1098/rspa.1982.0088.

Godoi, F.C., Prakash, S., Bhandari, B.R., 2016. 3d printing technologies applied for food design: status and prospects. J. Food Eng. 179, 44–54. https://doi.org/10.1016/j.jfoodeng.2016.01.025.

Godoi, F.C., Bhandari, B.R., Prakash, S., Zhang, M., 2019. An introduction to the principles of 3D food printing. In: Fundamentals of 3D Food Printing and Applications. Elsevier Inc. https://doi.org/10.1016/b978-0-12-814564-7.00001-8.

Han, X., Ding, S., Lu, J., Li, Y., 2022. Global, regional, and national burdens of common micronutrient deficiencies from 1990 to 2019: a secondary trend analysis based on the Global Burden of Disease 2019 study. https://doi.org/10.1016/j.

Huang, J.H.R., Lim, G.G.C.W., Su, C. H. Joan, Ciou, J.Y., 2023. Improvement of 3D white chocolate printing molding effect with oleogels. Heliyon 9 (9), e19165. https://doi.org/10.1016/j.heliyon.2023.e19165.

Ji, S., Xu, T., Li, Y., Li, H., Zhong, Y., Lu, B., 2022. Effect of starch molecular structure on precision and texture properties of 3D printed products. Food Hydrocolloids 125. https://doi.org/10.1016/j.foodhyd.2021.107387.

Jiang, J., Zeng, J., Gao, H., Zhang, L., Wang, F., Su, T., Xiang, F., Li, G., 2020. Effect of low temperature on the aging characteristics of a potato starch gel. Int. J. Biol. Macromol. 150, 519–527. https://doi.org/10.1016/j.ijbiomac.2020.02.077.

Kadival, A., Kour, M., Meena, D., Mitra, J., 2023. Extrusion-based 3D food printing: printability assessment and improvement techniques. In: Food and Bioprocess Technology, vol. 16. Springer, pp. 987–1008. https://doi.org/10.1007/s11947-022-02931-z, 5.

Kim, H.W., Bae, H., Park, H.J., 2017. Classification of the printability of selected food for 3D printing: development of an assessment method using hydrocolloids as reference material. J. Food Eng. 215, 23–32. https://doi.org/10.1016/j.jfoodeng.2017.07.017.

Kong, D., Zhang, M., Mujumdar, A.S., Li, J., 2023. Feasibility of hydrocolloid addition for 3D printing of Qingtuan with red bean filling as a dysphagia food. Food Res. Int. 165. https://doi.org/10.1016/j.foodres.2023.112469.

Krokida, M.K., Maroulis, Z.B., Saravacos, G.D., 2001. Rheological properties of fluid fruit and vegetable puree products: compilation of literature data. Int. J. Food Prop. 4 (2), 179–200. https://doi.org/10.1081/JFP-100105186.

Latham, M., 2002. Nutrición humana en el mundo en desarrollo. In: FAO: Alimentación Y Nutrición; 29, 1vol; 508pp; 24cms. FAO, Roma, 92-5-303818-7.

Lee, E.J., Hong, G.P., 2023. Effect of the double heating cycle on the thermal gelling properties of vicilin fractions from soy, mung bean, red bean and their mixture with soy glycinin. Food Hydrocolloids 137. https://doi.org/10.1016/j.foodhyd.2022.108370.

Lee, J., 2021. A 3d food printing process for the new normal era: a review. In: Processes, vol. 9. MDPI. https://doi.org/10.3390/pr9091495. Issue 9.

Lin, Y.J., Punpongsanon, P., Wen, X., Iwai, D., Sato, K., Obrist, M., Mueller, S., 2020. FoodFab: creating food perception illusions using food 3D printing. Conference on Human Factors in Computing Systems - Proceedings. https://doi.org/10.1145/3313831.3376421.

Ling, K.C.L., Yee, A.Z.H., Leo, C.H., Chua, C.K., 2022. Understanding 3D food printing technology: an affordance approach. Mater. Today: Proc. 70, 622–626. https://doi.org/10.1016/j.matpr.2022.08.564.

Lipton, J.I., Lipson, H., Lipton, J., Arnold, D., Nigl, F., Lopez, N., Cohen, D., Norén, N., 2010. Multi-material food printing with complex internal structure suitable for conventional post-processing MUTLI-MATERIAL FOOD PRINTING WITH COMPLEX INTERNAL STRUCTURE SUITABLE FOR CONVENTIONAL POST-PROCESSING. https://www.researchgate.net/publication/266588628.

Liu, L., Meng, Y., Dai, X., Chen, K., Zhu, Y., 2019. 3D printing complex egg white protein objects: properties and optimization. Food Bioprocess Technol. 12 (2), 267–279. https://doi.org/10.1007/s11947-018-2209-z.

Mantihal, S., Prakash, S., Godoi, F.C., Bhandari, B., 2019. Effect of additives on thermal, rheological and tribological properties of 3D printed dark chocolate. Food Res. Int. 119, 161–169. https://doi.org/10.1016/j.foodres.2019.01.056.

Marley, A., Brookes, M.J., 2023. Iron deficiency anaemia e modern investigation and management.

Martínez-Monzó, J., Cárdenas, J., García-Segovia, P., 2019. Effect of temperature on 3D printing of commercial potato puree. Food Biophys. 14 (3), 225–234. https://doi.org/10.1007/s11483-019-09576-0.

Matas, A., Igual, M., García-Segovia, P., Martínez-Monzó, J., 2022. Application of 3D printing in the design of functional gluten-free dough. Foods 11 (11), 1555. https://doi.org/10.3390/foods11111555.

Matas, A., Molina-Montero, C., Igual, M., García-Segovia, P., Martínez-Monzó, J., 2023. Viability study on the use of three different gels for 3D food printing. Gels 9 (9). https://doi.org/10.3390/gels9090736.

Mirazimi, F., Saldo, J., Sepulcre, F., Gràcia, A., Pujola, M., 2022. Enriched puree potato with soy protein for dysphagia patients by using 3D printing. Food Frontiers 3 (4), 706–715. https://doi.org/10.1002/fft2.149.

Mohamad, R., Agus, B.A.P., Hussain, N., 2019. Changes of phytosterols, rheology, antioxidant activity and emulsion stability of salad dressing with cocoa butter during storage. Food Technol. Biotechnol. 57 (1), 59–67. https://doi.org/10.17113/ftb.57.01.19.5692.

Molina-Montero, C., Vicente-Jurado, D., Igual, M., Martínez-Monzó, J., García-Segovia, P., 2023. Fiber enrichment of 3D printed apricot gel snacks with orange by-products. Gels 9 (7). https://doi.org/10.3390/gels9070569.

Nachal, N., Moses, J.A., Karthik, P., Anandharamakrishnan, C., 2019. Applications of 3D printing in food processing. In: Food Engineering Reviews, vol. 11. Springer, New York LLC, pp. 123–141. https://doi.org/10.1007/s12393-019-09199-8, 3.

Nijdam, J.J., Agarwal, D., Schon, B.S., 2022. An experimental assessment of filament-extrusion models used in slicer software for 3D food-printing applications. J. Food Eng. 317. https://doi.org/10.1016/j.jfoodeng.2021.110711.

Nijdam, J.J., LeCorre-Bordes, D., Delvart, A., Schon, B.S., 2021. A rheological test to assess the ability of food inks to form dimensionally stable 3D food structures. J. Food Eng. 291. https://doi.org/10.1016/j.jfoodeng.2020.110235.

ONU, 2015. THE 17 GOALS. United Nations. https://sdgs.un.org/goals.

Ortega Quintana, F.A., Galvan, E.S., Arrieta Rivero, R., Torres Gallo, R., 2015. Efecto de la temperatura y concentración sobre las propiedades reológicas de la pulpa de mango variedad Tommy Atkins. Revista ION 28 (2), 79–92. https://doi.org/10.18273/revion.v28n2-2015007.

Paxton, N.C., Zhao, J., Sauret, E., 2024. Polymer 3D printing in perspective: assessing challenges and opportunities in industrial translation against the metal benchmark. Int. J. Adv. Des. Manuf. Technol. https://doi.org/10.1007/s00170-024-13744-z.

Pereira, T., Barroso, S., Gil, M.M., 2021. Food texture design by 3d printing: a review. In: Foods, vol. 10. MDPI AG. https://doi.org/10.3390/foods10020320. Issue 2.

Pure, A.E., Yarmand, M.S., Farhoodi, M., Adedeji, A., 2021. Microwave treatment to modify textural properties of high protein gel applicable as dysphagia food. J. Texture Stud. 52 (5–6), 638–646. https://doi.org/10.1111/jtxs.12611.

Qiu, L., Zhang, M., Adhikari, B., Lin, J., Luo, Z., 2024. Preparation and characterization of 3D printed texture-modified food for the elderly using mung bean protein, rose powder, and flaxseed gum. J. Food Eng. 361. https://doi.org/10.1016/j.jfoodeng.2023.111750.

Rahman, J.M.H., Shiblee, M.N.I., Ahmed, K., Khosla, A., Kawakami, M., Furukawa, H., 2020a. Rheological and mechanical properties of edible gel materials for 3D food printing technology. Heliyon 6 (12), e05859. https://doi.org/10.1016/j.heliyon.2020.e05859.

Rahman, J.M.H., Shiblee, M.N.I., Ahmed, K., Khosla, A., Kawakami, M., Furukawa, H., 2020b. Rheological and mechanical properties of edible gel materials for 3D food printing technology. Heliyon 6 (12), e05859. https://doi.org/10.1016/j.heliyon.2020.e05859.

Ramakrishnan, U., 2002. Prevalence of micronutrient malnutrition worldwide. Nutr. Rev. 60 (5). https://academic.oup.com/nutritionreviews/article/60/suppl_5/S46/1896146.

Ricci, I., Derossi, A., Severini, C., 2018. 3D printed food from fruits and vegetables. In: Fundamentals of 3D Food Printing and Applications. Elsevier, pp. 117–149. https://doi.org/10.1016/B978-0-12-814564-7.00005-5.

Sandhu, K., Singh, S., 2022. Food printing: 3D printing in food industry. In: Food Printing: 3D Printing in Food Industry. Springer Nature. https://doi.org/10.1007/978-981-16-8121-9.

Sehgal, S., Singh, B., Sharma, V., 2022. Smart and sustainable food technologies. In: Smart and Sustainable Food Technologies. Springer Nature. https://doi.org/10.1007/978-981-19-1746-2.

Severini, C., Derossi, A., Azzollini, D., 2016. Variables affecting the printability of foods: preliminary tests on cereal-based products. Innovative Food Sci. Emerging Technol. 38, 281–291. https://doi.org/10.1016/j.ifset.2016.10.001.

Sharma, R., Chandra Nath, P., Kumar Hazarika, T., Ojha, A., Kumar Nayak, P., Sridhar, K., 2024. Recent advances in 3D printing properties of natural food gels: application of innovative food additives. In: Food Chemistry, vol. 432. Elsevier Ltd. https://doi.org/10.1016/j.foodchem.2023.137196.

Shi, Y., Zhang, M., Bhandari, B., 2021. Effect of addition of beeswax based oleogel on 3D printing of potato starch-protein system. Food Struct. 27. https://doi.org/10.1016/j.foostr.2021.100176.

Souza, J., Sousa, B., Augusto, P., Esteves, P., Paula, A., Chieregato, B., 2024. 3D food printing: fundamental concepts, crucial factors, and A critical discussion about acceptance and sustainable. In: Jacob-Lopes, E., Quiroz, L., Costa, M. (Eds.), SMART FOOD INDUSTRY :The Blockchain for Sustainable Engineering Volume II - Current Status, Future Foods, and Global Issues, 1 ed., vol. 2. CRC Press, pp. 185–210.

Tang, G.H., Sholzberg, M., 2024. Iron deficiency anemia among women: an issue of health equity. In: Blood Reviews, vol. 64. Churchill Livingstone. https://doi.org/10.1016/j.blre.2023.101159.

Thangalakshmi, S., Arora, V.K., Prithviraj, V., 2021. A comprehensive assessment of 3D food printing: technological and processing aspects. In: Journal of Biosystems Engineering, vol. 46. Springer Science and Business Media Deutschland GmbH, pp. 286–304. https://doi.org/10.1007/s42853-021-00106-w, 3.

Thangalakshmi, S., Arora, V.K., 2022. Three-Dimensional (3D) food printing and its process parameters. In: Sandhu, K., Singh, S. (Eds.), Food Printing: 3D Printing in Food Industry. Springer, Singapore. https://doi.org/10.1007/978-981-16-8121-9_3.

Tian, H., Wang, K., Qiu, R., Wang, S., Hu, Z., Zhao, L., 2022. Effects of incubation temperature on the mechanical and structure performance of beeswax-carrageenan-xanthan hybrid gelator system in 3D printing. Food Hydrocolloids 127. https://doi.org/10.1016/j.foodhyd.2022.107541.

Uribe-Wandurraga, Z.N., Zhang, L., Noort, M.W.J., Schutyser, M.A.I., García-Segovia, P., Martínez-Monzó, J., 2020. Printability and physicochemical properties of microalgae-enriched 3D-printed snacks. https://doi.org/10.1007/s11947-020-02544-4/Published.

Varvara, R.A., Szabo, K., Vodnar, D.C., 2021. 3D food printing: principles of obtaining digitally-designed nourishment. In: Nutrients, vol. 13. MDPI. https://doi.org/10.3390/nu13103617. Issue 10.

Wang, D., Zhang, T., Guo, X., Ling, D., Hu, L., Jiang, G., 2023. The potential of 3D printing in facilitating carbon neutrality. J. Environ. Sci. (China) 130, 85–91. https://doi.org/10.1016/j.jes.2022.10.024.

Wang, L., Zhang, M., Bhandari, B., Yang, C., 2018. Investigation on fish surimi gel as promising food material for 3D printing. J. Food Eng. 220, 101–108. https://doi.org/10.1016/j.jfoodeng.2017.02.029.

Wang, R., Hartel, R.W., 2021. Understanding stickiness in sugar-rich food systems: a review of mechanisms, analyses, and solutions of adhesion. Compr. Rev. Food Sci. Food Saf. 20 (6), 5901–5937. https://doi.org/10.1111/1541-4337.12833.

Waseem, M., Tahir, A.U., Majeed, Y., 2023. Printing the future of food: the physics perspective on 3D food printing. Food Physics 1, 100003. https://doi.org/10.1016/j.foodp.2023.100003.

Wedamulla, N.E., Fan, M., Choi, Y.J., Kim, E.K., 2023. Effect of pectin on printability and textural properties of potato starch 3D food printing gel during cold storage. Food Hydrocolloids 137. https://doi.org/10.1016/j.foodhyd.2022.108362.

World Health Organization (WHO), 2024. Micronutrients. World Health Organization. https://www.who.int/health-topics/micronutrients#tab=tab_1.

Yu, N., Yang, F., Gong, H., Zhou, J., Jie, C., Wang, W., Chen, X., Sun, L., 2022. Gel & three-dimensional printing properties of sheep plasma protein-surimi induced by transglutaminase. J. Food Eng. 323. https://doi.org/10.1016/j.jfoodeng.2022.111006.

Zhang, J., Li, Y., Cai, Y., Ahmad, I., Zhang, A., Ding, Y., Qiu, Y., Zhang, G., Tang, W., Lyu, F., 2022. Hot extrusion 3D printing technologies based on starchy food: a review. In: Carbohydrate Polymers, vol. 294. Elsevier Ltd. https://doi.org/10.1016/j.carbpol.2022.119763.

Zhou, L., Meng, F.B., Li, Y.C., Shi, X.D., Yang, Y.W., Wang, M., 2023. Effect of peach gum polysaccharide on the rheological and 3D printing properties of gelatin-based functional gummy candy. Int. J. Biol. Macromol. 253. https://doi.org/10.1016/j.ijbiomac.2023.127186.

Zhagal, M.C., Scanlon, H.D., Sapirstein, H.D., 2002. Cellular Structure of bread crumb and its influence on mechanical properties. J. Cereal. Sci. 36. https://doi.org/10.1006/jcrs.2001.0445.